Article

# Emergence of a distinct mechanism of C–N bond formation in photoenzymes

https://doi.org/10.1038/s41586-024-08138-w

Received: 16 April 2024

Accepted: 30 September 2024

Published online: 8 October 2024

Check for updates

Felix C. Raps[1,2], Ariadna Rivas-Souchet[1,2], Chey M. Jones[3] & Todd K. Hyster[1,2]✉

C–N bond formation is integral to modern chemical synthesis owing to the ubiquity of nitrogen heterocycles in small-molecule pharmaceuticals and agrochemicals. Alkene hydroamination with unactivated alkenes is an atom-economical strategy for constructing these bonds. However, these reactions are challenging to render asymmetric when preparing fully substituted carbon stereocentres. Here we report a photoenzymatic alkene hydroamination to prepare 2,2-disubstituted pyrrolidines by a Baeyer–Villiger mono-oxygenase. Five rounds of protein engineering afforded a mutant, providing excellent product yield and stereoselectivity. Unlike related photochemical hydroaminations, which rely on the oxidation of the amine or alkene for C–N bond formation, this work exploits a through-space interaction of a reductively generated benzylic radical and the nitrogen lone pair. This antibonding interaction lowers the oxidation potential of the radical, enabling electron transfer to the flavin cofactor. Experiments indicate that the enzyme microenvironment is essential in enabling a innovative C–N bond formation mechanism with no parallel in small-molecule catalysis. Molecular dynamics simulations were performed to investigate the substrate in the enzyme active site, which further support this hypothesis. This work is a rare example of an emerging mechanism in non-natural biocatalysis in which an enzyme has access to a mechanism that its individual components do not. Our study showcases the potential of enhancing emergent mechanisms using protein engineering to provide unique mechanistic solutions to unanswered challenges in chemical synthesis.

Enzymes are ideal scaffolds for chemical synthesis because they use an ensemble of covalent and non-covalent interactions between reactive intermediates and the protein to facilitate transformations[1]. These contacts enable enzymes to carry out transformations with unparalleled levels of selectivity and perform reaction mechanisms that are inaccessible to cofactors or minimalist proteins[2]. A complex system with access to mechanisms in which individual parts do not display a property is known as emergence[3]. The phenomenon of emerging mechanisms is well known for native enzyme function but is rare when using enzymes for non-natural reactivity[4–7]. Examples include P411-catalysed nitrene insertion into C–H bonds and bicyclobutane formation[8], higher-order charge transfer complexes with flavin-dependent oxidoreductases[9] and mesolytic cleavage of nitroradical anions in reductive couplings using 'ene' reductases[10]. Although emerging mechanisms are challenging to predict, when discovered and optimized using protein engineering, they have the potential to unlock new reactions and retrosynthetic disconnections[11].

Hydroamination of alkenes with unactivated amines is an atom-economical strategy for constructing new C–N bonds[12,13]. These seemingly simple transformations are, however, challenging to implement when moving beyond model substrates. For example, the asymmetric construction of α-tertiary amines by coupling 1,1-disubstituted alkenes with amines through a Markovnikov hydroamination remains a substantial challenge[14]. Transition metals, the most common hydroamination catalysts, are poorly suited for constructing sterically hindered bonds[15,16]. Reactions involving radical intermediates are functional group tolerant, but form exclusively the anti-Markovnikov product and are challenging to render asymmetric in the C–N-bond-forming event[17] (Fig. 1a). By contrast, Brønsted acid catalysts were recently reported to catalyse this transformation but have poor functional group tolerance and require deactivated amines with directing groups to achieve enantioselectivity[18]. We envisioned enzymes to be ideally suited for this type of reaction. However, there are no known biocatalysts capable of catalysing hydroaminations with unactivated amines and alkenes. Given their high reactivity, compatibility with aqueous conditions and substrate tolerance, we envisioned radicals as ideal intermediates for the desired reaction. However, the enzyme will need to use a unique mechanism to override the inherent regioselectivity of the known radical mechanisms of C–N bond formation.

We targeted the development of an enzyme-catalysed intramolecular hydroamination to prepare 2,2-disubstituted pyrrolidines (Fig. 1b). Our group and others have demonstrated that flavin-dependent ene-reductases can catalyse various reactions that form C–C

[1]Department of Chemistry, Princeton University, Princeton, NJ, USA. [2]Department of Chemistry and Chemical Biology, Cornell University, Ithaca, NY, USA. [3]Merck & Co., Inc., Rahway, NJ, USA. ✉e-mail: thyster@princeton.edu

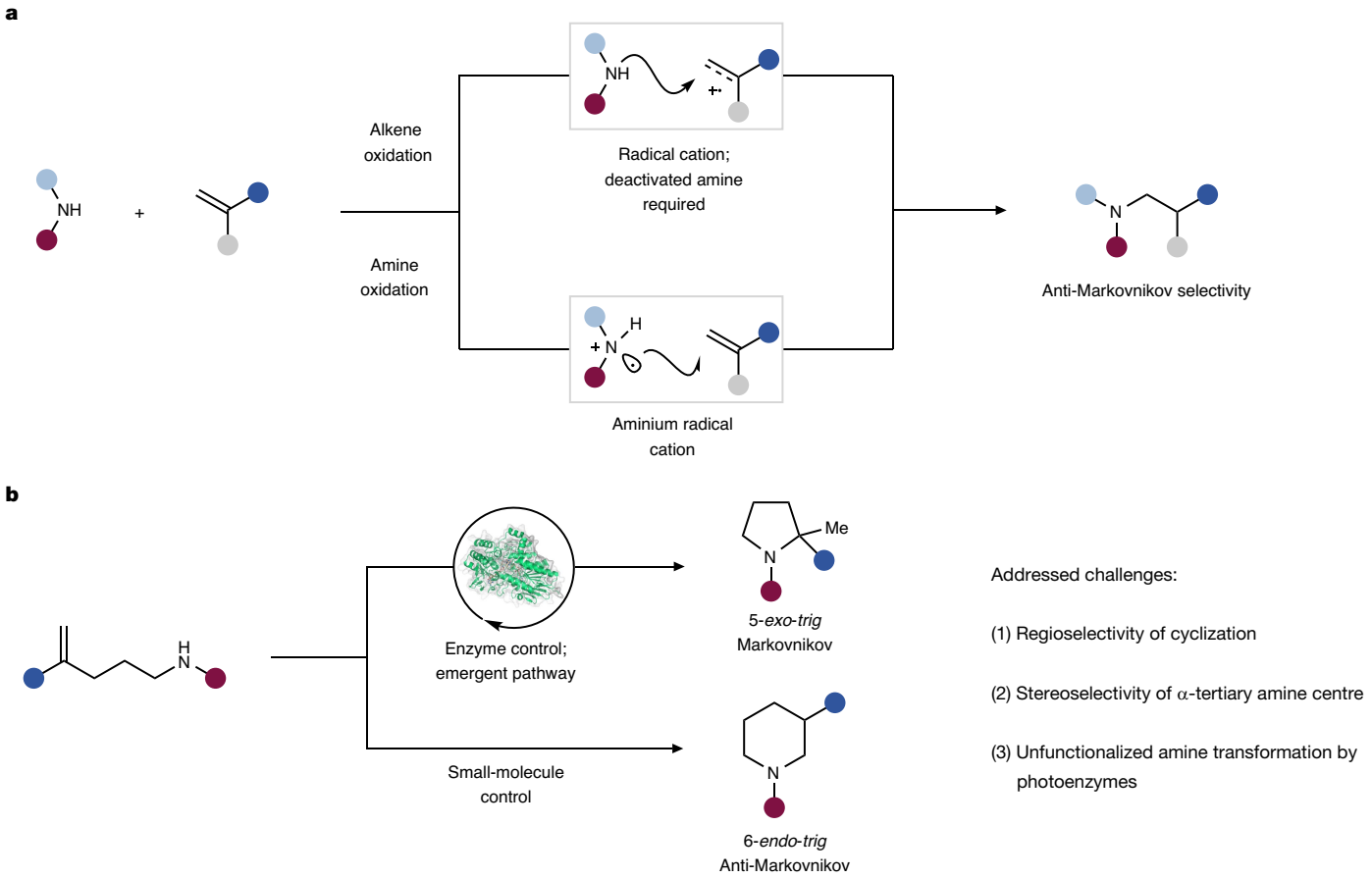


**Fig. 1 | Challenges in radical hydroaminations. a**, Small-molecule-catalysed radical hydroamination strategies and limitations. **b**, Enzyme control can address outstanding challenges in radical hydroaminations through emergent pathways.

(refs. 10,19–22), N–C (refs. 23,24) and C–O (ref. 25) bonds with regio- and enantioselectivities that can be tuned using protein engineering. A common feature of these reactions is the need for activated radical precursors, such as alkyl halides and hydroxamic esters, which—on reduction—undergo an irreversible bond cleavage to ensure that productive chemistry is competitive with back electron transfer. In this study, we targeted a photoenzymatic process that involves unactivated radical precursors, a challenge that needs to be overcome to increase the synthetic use of photoenzymatic processes.

We began by exploring the radical cyclization with model substrate **1** based on its ability to form products through a 5-*exo-trig* or 6-*endo-trig* cyclization (Fig. 2a). A library of flavoenzymes was compiled based on the hypothesis that an enzyme that naturally catalyses an oxidative transformation would best tolerate the anticipated radicals generated in the active site[6,26]. We found that monoamine oxidase (MAO-N-D11C)[27], styrene mono-oxygenase (StyA1)[28], D-amino acid oxidase (*Ac*DAAO)[29], choline oxidase (*Ac*CO6)[30] and cholesterol oxidase (*Sh*CO)[31] were unable to cyclize a hydroamination reaction when irradiated with blue light. By contrast, a cyclohexanone mono-oxygenase from *Acinetobacter calcoaceticus* (*Ac*CHMO) showed low conversion to 5-*exo-trig* hydroamination product **2** (1% yield, 55:45 enantiomeric ratio (e.r.)) without forming 6-*endo-trig* product **3**, the product formed when using aminyl or aminium radical cations[32] (Supplementary Fig. 6). Control experiments confirmed that CHMO and light were necessary for reactivity and that free flavin adenine dinucleotide (FAD) could not facilitate this transformation. To improve this activity, we built a library of CHMO homologues and found that a previously reported omeprazole sulfoxidase (*Ac*CHMO-M10) afforded product with a 12% yield and 55:45 e.r. (refs. 33–35).

With the initial activity in hand, we engaged in a protein-engineering campaign using iterative site saturation mutagenesis following a reduced codon strategy to increase the yield and enantioselectivity of the reaction[6,7,36]. Sites for mutagenesis were selected based on their proximity to the cofactor. To aid in selecting the sites for mutagenesis, we used a structure predicted by AlphaFold 2.0 that was modelled onto a crystal structure of ancestor *Ac*CHMO-M2 (Protein Data Bank (PDB) ID: 6A37)[35,37]. We began by targeting residues in 4 Å of the flavin cofactor (Fig. 2b,c). Substitution of arginine at position 327 to lysine (R327K) increased the yield to 22% with 71:29 e.r. Further rounds of mutagenesis identified sequential substitutions R490E (45%, 70:30 e.r.), C326H (56%, 81:19 e.r.) and I491T (71%, 93:7 e.r.). All three positions are situated in the substrate channel leading to the active site, presumably tailoring the position of the substrate during the reaction. Finally, the substitution of alanine at position 479 to histidine (A479H) led to product formation with a high yield and excellent enantioselectivity (97%, 95:5 e.r.). Molecular dynamics (MD) simulations reveal that the three distal substitutions—R490E, I491T and A479H—reside in a dynamic-loop region (residues 475–510) that gates access to the active site of the enzyme (Fig. 2d). This loop resembles the control-loop region that was investigated in homologous *Rm*CHMO[38] from *Rhodococcus*. In the parent enzyme, this flexible loop forms interactions (for example, between R490 and Q210) that close the active site entrance. The introduction of these distal substitutions appears to disrupt interactions between the active-site gating loop and other regions of the enzyme, which prevents the loop from shielding the active site. Thus, it is likely that the R490E, I491T and A479H substitutions play an important part in keeping the active site open and accessible to substrates—a plausible explanation for

**a**

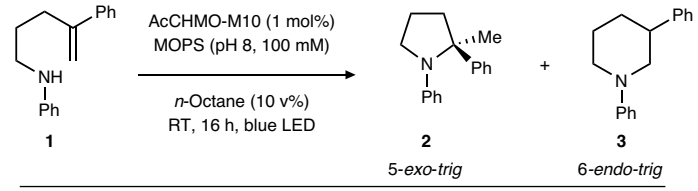


| Entry | Deviation | 5-*exo*-*trig* | e.r. |
|---|---|---|---|
| 1 | – | 12% | 55:45 |
| 2 | Engineered enzyme | 97% | 95:5 |
| 3 | Lysate (0.04 mol%) | 15% | 95:5 |
| 4 | FAD | – | – |
| 5 | No light | – | – |
| 6 | No enzyme | – | – |

**b**

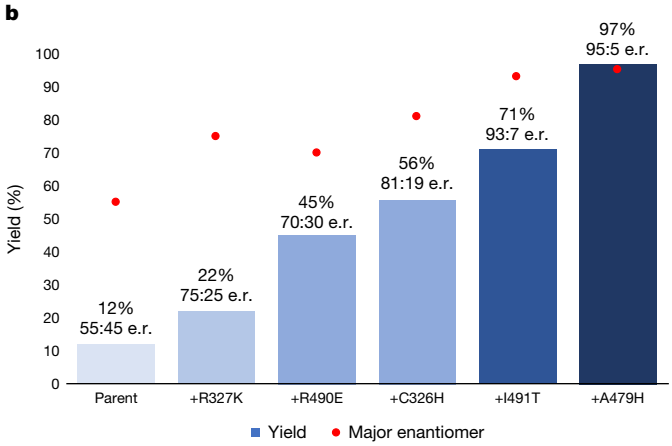


**c**

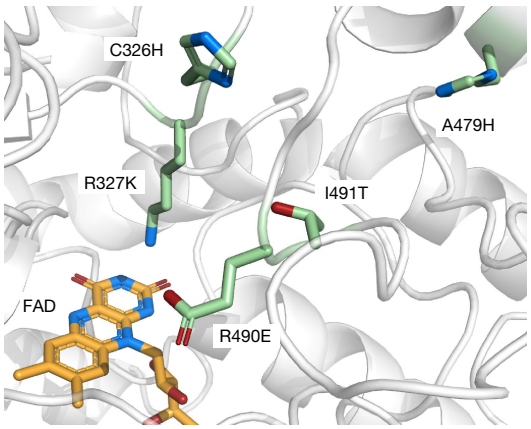


**d**

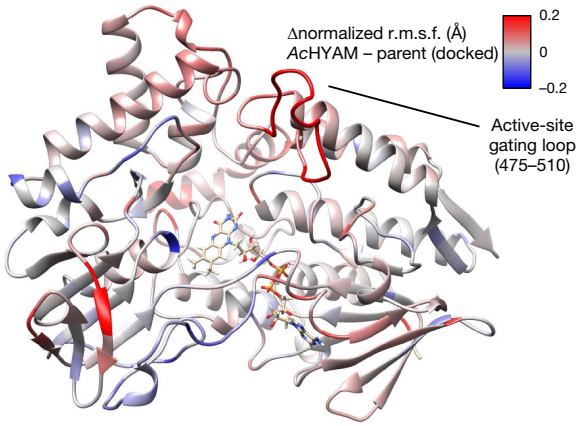


**Fig. 2 | Protein evolution. a**, Model reaction for selective photoenzymatic hydroamination. RT, room temperature; MOPS, (3-(*N*-morpholino) propanesulfonic acid). **b**, Overview of evolution campaign and increments in yield and enantioselectivity. **c**, Protein structure of *Ac*HYAM is shown; the structure was predicted using AlphaFold 2.0 and aligned to the crystal structure of ancestor *Ac*CHMO-M2 (PDB ID: 6A37)[35,54]. **d**, Difference in residue root mean square fluctuations (r.m.s.f.) between the parent and *Ac*HYAM MD simulations indicate the loss of salt bridges in the active-site gating loop. For each docked enzyme, per-residue r.m.s.f. values were calculated from the MD simulations and normalized between 0 (that is, the least flexible residues) and 1 (that is, the most flexible residues). To highlight regions with the largest changes in structural flexibility, the difference between these normalized values was calculated as well (that is, Δnormalized r.m.s.f.). Negative (blue) values indicate regions where *Ac*HYAM is more rigid than the parent enzyme, whereas positive (red) values indicate regions where *Ac*HYAM is more flexible than the parent enzyme.

the approximate 15–30% yield improvements associated with these substitutions.

The efficacy of the enzyme to catalyse the reaction was tested in cell-free dialysed lysate by lowering the catalyst loading to 0.04 mol% (Fig. 2a, entry 3). The reaction still proceeded in modest amounts (17%, turnover number = 436), forming product **4** and retaining the e.r. value. In the undialysed lysate (1 mol%), we observed a diminished e.r. value (93:7) of the product. When considering possible inhibitors, we recognized $NADP^+$ as a potential candidate based on its role in the natural mechanism[34]. When 0.1 equiv. of $NADP^+$ relative to the enzyme was added to the reaction, the yield decreased to 63% with a decrease in enantioselectivity to 93:7 e.r. Addition of equimolar amounts of $NADP^+$ to enzyme (1.0 equiv. of $NADP^+$ relative to the enzyme) entirely impedes the reaction, suggesting that $NADP^+$ binding is inhibitory. This is distinct from the native reactivity, which requires both FADH and $NADP^+$ (ref. 34).

The final enzyme—called *A. calcoaceticus* hydroaminase (*Ac*HYAM)—was tested for its proficiency in catalysing the cyclization on several substrates (Fig. 3). Various aniline and styryl substitutions were tolerated, with electron-rich arenes generally affording higher yields and selectivity (**2**, **4**–**10** and **13**–**20**). Large substituents, such as naphthalenes, on the aniline side (**10**) and the styrene moiety (**19**) did not diminish the yield and were transformed with excellent enantioselectivities. Moreover, electron-deficient nitrogen-containing heterocycles are tolerated (**11**, **12** and **21**), overcoming a limitation to Brønsted-acid-catalysed cyclization. The cyclization was sensitive to the heterocyclic substitution and was severely hampered in some cases (Supplementary Fig. 1). Nevertheless, protein engineering might overcome these limitations. The homologated substrate can engage in a 6-*exo*-*trig* cyclization to afford product **22** with a 13% yield and promising levels of enantioselectivity (78:22 e.r.). This particular example is fascinating, because, when using a photoredox catalyst, this type of substrate could typically undergo a 1,5-hydrogen-atom transfer event over cyclization[39]. Modifications to the backbone of the pyrrolidines were tolerated with dimethyl substitution **23** obtained with a moderate yield (42%) and e.r. (27:73).

Next, we used this method to prepare the α-methylated analogue of three aryl-pyrrolidine-containing active pharmaceutical ingredients (APIs). The methylated pyrrolidine fragment of TRK inhibitor GNF-8625 (ref. 40) was obtained with an excellent yield (**24**; 85%, 94:6 e.r.), as well as the fragments of the modified tropomyosin inhibitor α-methyl larotrectinib (**26**; 77%, 75:25 e.r.)[41] and related structure (**25**; 25%, 73:27 e.r.)[42]. These syntheses demonstrate the ease with which

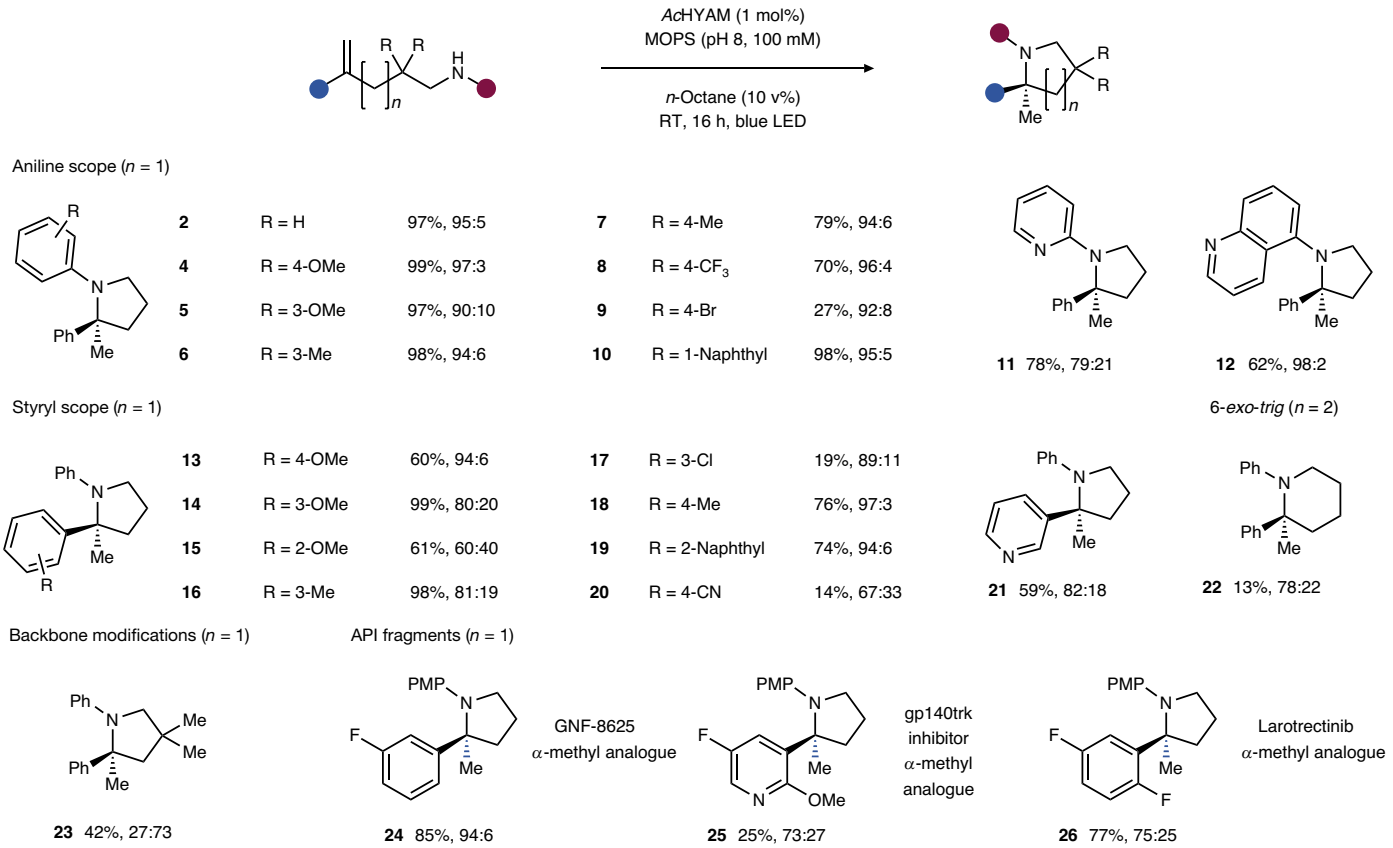


**Fig. 3 | Scope of C–N-forming reaction.** Substrate scope of the photoenzymatic hydroamination reaction. Modifications are separated into aniline and styryl modifications, as well as other distinct modifications. PMP, *para*-methoxyphenyl.

this method can prepare substituted analogues that typically involve multistep sequences.

Next, we investigated the mechanism of the reaction. At the onset, we hypothesized that an enzymatic hydroamination would initiate the reaction through substrate oxidation. However, the observation of an induction period suggested that oxidized flavin is not responsible for radical initiation. Instead, it needs to be photoreduced for the reaction to occur (Supplementary Fig. 2). To determine whether a reduced oxidation state of flavin was responsible for radical initiation, we ran the model reaction with the enzyme pre-reduced by sodium dithionite and observed product formation with a 74% yield and 95:5 e.r. and the induction period was lost[43] (Supplementary Fig. 3). Importantly, the ultraviolet–visible spectrum produced when the enzyme is reduced by dithionite is identical to the one observed when the enzyme is photoreduced by a buffer, indicating that both conditions produce the same flavin oxidation state (Supplementary Figs. 4 and 5). These results reveal that the observed induction period was because the photoreduction[44] of FAD to $FAD_{hq}$ was required, indicating that the reaction initiates from the reduced form of the cofactor. These results exclude a nitrogen-centred radical as the reactive intermediate, as only an oxidizing photocatalyst could form this species. Indeed, when aniline **1** is subjected to reaction conditions for generating aminium radical cations known from literature, only the product of a 6-*exo-trig* cyclization is observed, inconsistent with the results from the enzymatic reaction[45] (Supplementary Fig. 6).

Next, we considered whether reduced flavin was serving as an energy transfer catalyst[46]. A previous study has described 5-*exo-trig* hydroamination by direct excitation at 281 nm in the absence of a photocatalyst[47] (Supplementary Fig. 7). In this study, the researchers proposed that a diradical combination is responsible for the bond-forming event and substantiated their hypothesis by observing fragmentation in a derivative substrate. To probe any diradical character in the enzymatic reaction, a related fragmentation substrate (substrate **40** in the Supplementary Information) was subjected to the enzymatic reaction conditions, and samples were analysed using gas chromatography–mass spectrometry and nuclear magnetic resonance methods. No evidence for fragmentation was observed, suggesting that an energy transfer mechanism is unlikely.

Because of the need for reduced flavin and the lack of evidence for an energy transfer mechanism, we concluded that alkene reduction by $FAD_{hq}{}^*$ ($E^0 = -2.26$ V versus saturated calomel electrode (SCE)) is responsible for radical initiation[21] (Fig. 4a). Although this potential should not be sufficient to reduce the substrate (α-methyl styrene $E^{red} = -2.6$ V versus SCE)[48], the electropositive active site can attenuate the potential required to reduce the alkene as well as stabilize the resulting anionic flavin semiquinone[49] ($FAD_{sq}{}^-$) (Fig. 4b). The resulting radical anion is highly basic, leading to a fast and irreversible protonation and resulting in benzylic radical formation. Although we initially hypothesized that this radical is oxidized to the corresponding benzylic cation, substrates bearing other nucleophilic species, such as primary alcohol **27**, alkylamine **28** and methyl-substituted alkene derivative **29**, are completely unreactive (Fig. 4c). This observation is inconsistent with a tertiary carbocation and suggests that a π–π-stacking interaction is required for the reaction to proceed. When considering other mechanistic possibilities for C–N bond formation, we hypothesized that an interaction between the aniline and benzylic radical could alter the redox properties of the system. Even though this type of transannular interaction is unknown in the literature, it is well known that hyperconjugative interactions between lone pairs and radicals will increase the energy of the singly occupied molecular orbital, making the radical easier to oxidize[50]. If the protein were to template this interaction and

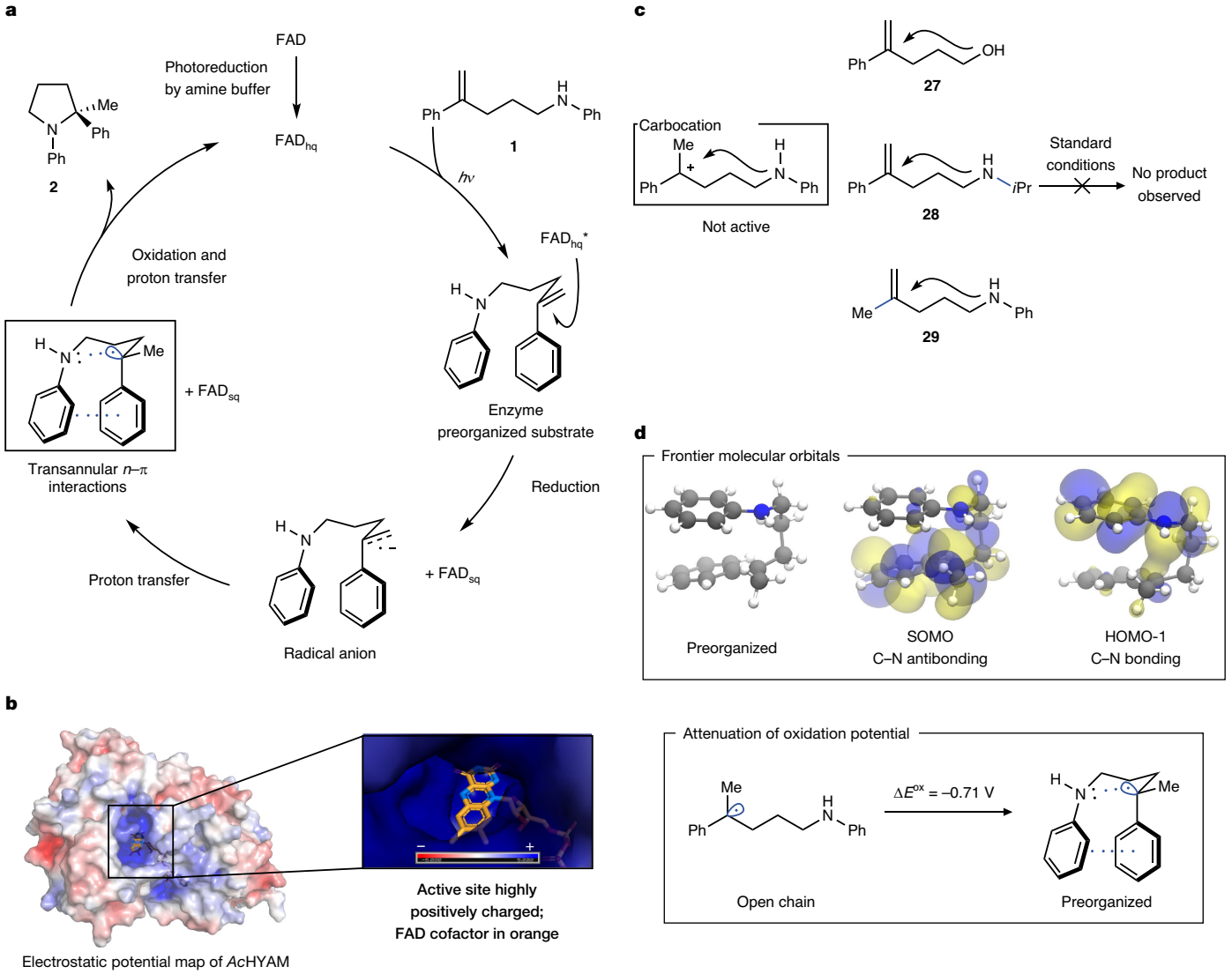


**Fig. 4 | Mechanistic investigations with substrate probes and DFT.** **a**, Proposed catalytic cycle in the hydroamination reaction. **b**, Adaptive Poisson–Boltzmann Solver (APBS)[55] calculated the electrostatic potential map of *Ac*HYAM, indicating a positively charged active site. **c**, Carbocation reactivity and substrates designed to probe any ionic-bond-forming activity. **d**, DFT calculations of the preorganized form in MeCN. Frontier molecular orbitals and energies were calculated at the M06-D3(0)/6-311+G(d,p) level of theory. Redox potentials were determined using the Born–Haber relation. HOMO-1, highest occupied molecular orbital-1; SOMO, singly occupied molecular orbital.

overcome the repulsive electronic forces by confining the substrate in a reactive conformer, a similar redox activation would be expected. We calculated the frontier molecular orbital configuration of the preorganized intermediate by density functional theory (DFT) (Fig. 4d). The prealigned structure was determined by performing a coordinate scan of the product in its doublet state. The C–N bond was pulled apart in iterations to identify an energetic minimum, which was optimized at the M06-D3(0)/6-311+G(d,p) level of theory[51]. The resulting singly occupied molecular orbital populates an antibonding configuration with the orbitals out of phase for C–N bond formation with strong character on the styrenyl arene. However, highest occupied molecular orbital-1 has bonding character between the aniline nitrogen and benzylic radical with marked orbital coefficients on the aniline arene, supporting our hypothesis that this type of $n \rightarrow$ singly occupied molecular orbital can lead to the bonding character. The oxidation potentials of the preorganized and open-chain structures were determined by DFT using the Born–Haber relation. The oxidation potential of the unaligned form closely matched the benzylic α-methyl styrenyl radical (Supplementary Fig. 8). In the calculated prealigned structure, the oxidation potential was found to be substantially lowered ($\Delta E^{ox} = -0.70$ V versus SCE). This feature is vital because $FAD_{sq}^{-}$ is insufficiently oxidizing ($E^0 = -0.25$ V versus SCE)[52] to produce a benzylic carbocation from the corresponding radical ($E^{ox} = 0.16$ V versus SCE)[50].

On the basis of the observed reactivity and gathered mechanistic evidence, we conclude that the enzyme facilitates this hydroamination using a mechanism that is distinct from that of small-molecule catalysis. This emergent mechanism relies on the repulsive interactions from a formal two-centre three-electron antibonding intermediate to attenuate the oxidation potential of the radical in the enzyme active site. We hypothesized that this interaction is only possible because of the preorganization provided by the protein. Surprisingly, MD simulations suggest that the *Ac*HYAM environment provides the model substrate with more rotational freedom relative to the parent enzyme. However, we see evidence of substrate conformations in *Ac*HYAM that resemble the preorganized conformation investigated by DFT (Fig. 5a), which are sparsely observed in the parent enzyme. Amino-acid substitutions near the catalytic site (that is, R327K and C326H) are probably responsible for this enhanced conformational flexibility, as the substrate

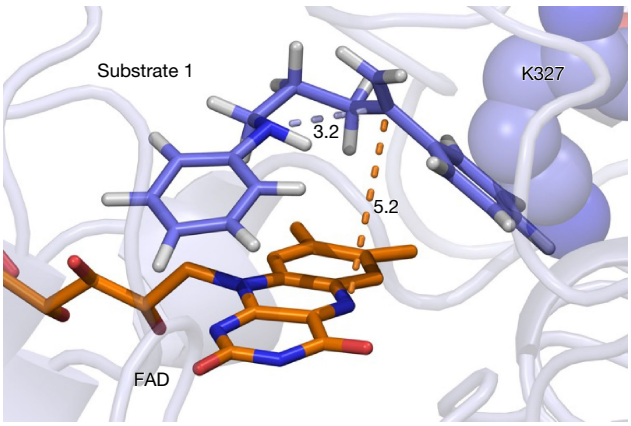


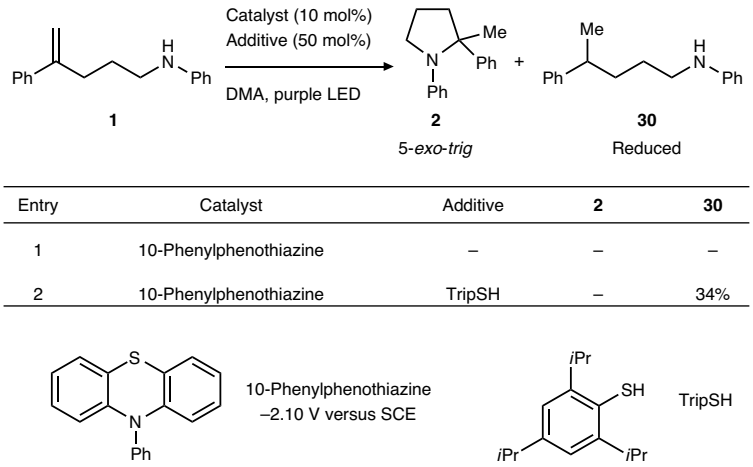


| Entry | Catalyst | Additive | 2 | 30 |
|---|---|---|---|---|
| 1 | 10-Phenylphenothiazine | – | – | – |
| 2 | 10-Phenylphenothiazine | TripSH | – | 34% |




10-Phenylphenothiazine
–2.10 V versus SCE




TripSH

**Fig. 5 | Investigations into substrate binding with MD simulations and small-molecule tests. a**, Snapshot of a model substrate conformation (light blue)—sampled during *Ac*HYAM MD simulations—that resembles the preorganized conformation investigated with DFT calculations. The distance between the radical-bearing carbon atom of the substrate and the specified FAD nitrogen atom is shown in orange. The distance between the radical-bearing carbon atom and nitrogen atom of the substrate is shown in light blue. The K327 residue is shown using spheres. **b**, Small-molecule photocatalysed transformations of the model substrate do not yield the enzymatic product. DMA, dimethylacetamide.

predominantly samples extended conformations in the parent enzyme. We concluded that the new rotational freedom enables the substrate in the engineered *Ac*HYAM environment to orient itself into the conformation crucial for C–N bond formation.

Indeed, when a photoredox reaction was conducted with 10-phenylphenothiazine, a photocatalyst reported to reduce α-methyl styrene to the corresponding radical anion[53], no 5-*exo-trig* product was observed (Fig. 5b). When the same reaction is conducted in the presence of a thiol catalyst, alkene reduction was found with a 34% yield, indicating that despite the ability of 10-phenylphenothiazine to reduce the alkene of **1** to the radical anion, no C–N bond formation occurs without the templating provided.

In conclusion, we have developed a highly selective photoenzyme for a stereoselective hydroamination using anilines. On the basis of experiments and calculations, we conclude that this reaction uses a previously unknown mechanism for C–N bond formation, which is enabled by the preorganization provided by the protein active site. This emergent mechanism of C–N bond formation highlights the opportunity for enzymes to reveal new pathways, which can be used to address reactivity challenges in chemical synthesis.

## Online content

Any methods, additional references, Nature Portfolio reporting summaries, source data, extended data, supplementary information, acknowledgements, peer review information; details of author contributions and competing interests; and statements of data and code availability are available at https://doi.org/10.1038/s41586-024-08138-w.


1. Knowles, J. R. Enzyme catalysis: not different, just better. *Nature* **350**, 121–124 (1991).
2. Zhang, X. et al. Divergent synthesis of complex diterpenes through a hybrid oxidative approach. *Science* **369**, 799–806 (2020).
3. Luisi, P. L. Emergence in chemistry: chemistry as the embodiment of emergence. *Found. Chem.* **4**, 183–200 (2002).
4. Brustad, E. M. & Arnold, F. H. Optimizing non-natural protein function with directed evolution. *Curr. Opin. Chem. Biol.* **15**, 201–210 (2011).
5. Renata, H., Wang, Z. J. & Arnold, F. H. Expanding the enzyme universe: accessing non-natural reactions by mechanism-guided directed evolution. *Angew. Chem. Int. Ed.* **54**, 3351–3367 (2015).
6. Arnold, F. H. Directed evolution: bringing new chemistry to life. *Angew. Chem. Int. Ed.* **57**, 4143–4148 (2018).
7. Chen, K. & Arnold, F. H. Engineering new catalytic activities in enzymes. *Nat. Catal.* **3**, 203–213 (2020).
8. Chen, K., Huang, X., Kan, S. B. J., Zhang, R. K. & Arnold, F. H. Enzymatic construction of highly strained carbocycles. *Science* **360**, 71–75 (2018).
9. Page, C. G. et al. Quaternary charge-transfer complex enables photoenzymatic intermolecular hydroalkylation of olefins. *J. Am. Chem. Soc.* **143**, 97–102 (2021).
10. Fu, H. et al. An asymmetric $sp^3$–$sp^3$ cross-electrophile coupling using 'ene'-reductases. *Nature* **610**, 302–307 (2022).
11. Zhao, Y. et al. The emergence of anion–π catalysis. *Acc. Chem. Res.* **51**, 2255–2263 (2018).
12. Molander, G. A. & Dowdy, E. D. Catalytic intramolecular hydroamination of hindered alkenes using organolanthanide complexes. *J. Org. Chem.* **63**, 8983–8988 (1998).
13. Müller, T. E., Hultzsch, K. C., Yus, M., Foubelo, F. & Tada, M. Hydroamination: direct addition of amines to alkenes and alkynes. *Chem. Rev.* **108**, 3795–3892 (2008).
14. Pratley, C., Fenner, S. & Murphy, J. A. Nitrogen-centered radicals in functionalization of $sp^2$ systems: generation, reactivity, and applications in synthesis. *Chem. Rev.* **122**, 8181–8260 (2022).
15. Huang, L., Arndt, M., Gooßen, K., Heydt, H. & Gooßen, L. J. Late transition metal-catalyzed hydroamination and hydroamidation. *Chem. Rev.* **115**, 2596–2697 (2015).
16. Xu, Y., Wang, J., Deng, G.-J. & Shao, W. Recent advances in the synthesis of chiral α-tertiary amines via transition-metal catalysis. *Chem. Commun.* **59**, 4099–4114 (2023).
17. Escorihuela, J., Lledós, A. & Ujaque, G. Anti-Markovnikov intermolecular hydroamination of alkenes and alkynes: a mechanistic view. *Chem. Rev.* **123**, 9139–9203 (2023).
18. Guria, S. et al. Enantioselective, Brønsted acid-catalyzed anti-selective hydroamination of alkenes. *J. Am. Chem. Soc.* **146**, 17180–17188 (2024).
19. Emmanuel, M. A. et al. Photobiocatalytic strategies for organic synthesis. *Chem. Rev.* **123**, 5459–5520 (2023).
20. Nicholls, B. T. et al. Engineering a non-natural photoenzyme for improved photon efficiency. *Angew. Chem. Int. Ed.* **61**, e202113842 (2022).
21. Biegasiewicz, K. F. et al. Photoexcitation of flavoenzymes enables a stereoselective radical cyclization. *Science* **364**, 1166–1169 (2019).
22. Sun, S.-Z. et al. Enantioselective decarboxylative alkylation using synergistic photoenzymatic catalysis. *Nat. Catal.* **7**, 35–42 (2024).
23. Ye, Y. et al. Using enzymes to tame nitrogen-centred radicals for enantioselective hydroamination. *Nat. Chem.* **15**, 206–212 (2022).
24. Zhang, Z. et al. Photoenzymatic enantioselective intermolecular radical hydroamination. *Nat. Catal.* **6**, 687–694 (2023).
25. Ouyang, Y., Turek-Herman, J., Qiao, T. & Hyster, T. K. Asymmetric carbohydroxylation of alkenes using photoenzymatic catalysis. *J. Am. Chem. Soc.* **145**, 17018–17022 (2023).
26. Packer, M. S. & Liu, D. R. Methods for the directed evolution of proteins. *Nat. Rev. Genet.* **16**, 379–394 (2015).
27. Batista, V. F. et al. Monoamine oxidase: tunable activity for amine resolution and functionalization. *ACS Catal.* **8**, 11889–11907 (2018).
28. Tischler, D. et al. StyA1 and StyA2B from *Rhodococcus opacus* 1CP: a multifunctional styrene monooxygenase system. *J. Bacteriol.* **192**, 5220–5227 (2010).
29. Pollegioni, L. & Molla, G. New biotech applications from evolved D-amino acid oxidases. *Trends Biotechnol.* **29**, 276–283 (2011).
30. Heath, R. S. et al. An engineered alcohol oxidase for the oxidation of primary alcohols. *ChemBioChem* **20**, 276–281 (2019).
31. Heath, R. S., Sangster, J. J. & Turner, N. J. An engineered cholesterol oxidase catalyses enantioselective oxidation of non-steroidal secondary alcohols. *ChemBioChem* **23**, e202200075 (2022).
32. Liu, F., Liu, K., Yuan, X. & Li, C. 5-*exo* versus 6-*endo* cyclization of primary aminyl radicals: an experimental and theoretical investigation. *J. Org. Chem.* **72**, 10231–10234 (2007).
33. Zhao, P. et al. Protein engineering of thioether monooxygenase to improve its thermostability for enzymatic synthesis of chiral sulfoxide. *Mol. Catal.* **509**, 111625 (2021).

34. Fürst, M. J. L. J., Gran-Scheuch, A., Aalbers, F. S. & Fraaije, M. W. Baeyer–Villiger monooxygenases: tunable oxidative biocatalysts. *ACS Catal.* **9**, 11207–11241 (2019).
35. Zhang, Y. et al. Engineering of cyclohexanone monooxygenase for the enantioselective synthesis of (*S*)-omeprazole. *ACS Sustain. Chem. Eng.* **7**, 7218–7226 (2019).
36. Reetz, M. T. Laboratory evolution of stereoselective enzymes: a prolific source of catalysts for asymmetric reactions. *Angew. Chem. Int. Ed.* **50**, 138–174 (2011).
37. Jumper, J. et al. Highly accurate protein structure prediction with AlphaFold. *Nature* **596**, 583–589 (2021).
38. Mirza, I. A. et al. Crystal structures of cyclohexanone monooxygenase reveal complex domain movements and a sliding cofactor. *J. Am. Chem. Soc.* **131**, 8848–8854 (2009).
39. Sarkar, S., Cheung, K. P. S. & Gevorgyan, V. C–H functionalization reactions enabled by hydrogen atom transfer to carbon-centered radicals. *Chem. Sci.* **11**, 12974–12993 (2020).
40. Liu, J., Plewe, M. B., Wang, J., Han, X. & Chen, L. Tropomyosin receptor kinase (TRK) degradation compounds and methods of use. US patent WO2020038415 (2019).
41. Min, J. et al. A kind of preparation method of larotrectinib and intermediate of larotrectinib. China patent CN107987082A (2017).
42. Allen, S. et al. Substituted pyrazolo[1,5-a]pyrimidine compounds as TRK kinase inhibitors. US patent WO2011006074 (2011).
43. Müller, F. & Massey, V. Flavin-sulfite complexes and their structures. *J. Biol. Chem.* **244**, 4007–4016 (1969).
44. Gonçalves, L. C. P. et al. Boosting photobioredox catalysis by morpholine electron donors under aerobic conditions. *Catal. Sci. Technol.* **9**, 2682–2688 (2019).
45. Ganley, J. M., Murray, P. R. D. & Knowles, R. R. Photocatalytic generation of aminium radical cations for C–N bond formation. *ACS Catal.* **10**, 11712–11738 (2020).
46. Strieth-Kalthoff, F., James, M. J., Teders, M., Pitzer, L. & Glorius, F. Energy transfer catalysis mediated by visible light: principles, applications, directions. *Chem. Soc. Rev.* **47**, 7190–7202 (2018).
47. Lewis, F. D., Bassani, D. M. & Reddy, G. D. Intramolecular photoaddition of secondary α-(aminoalkyl)styrenes. *J. Org. Chem.* **58**, 6390–6393 (1993).
48. Schreier, M. R., Pfund, B., Guo, X. & Wenger, O. S. Photo-triggered hydrogen atom transfer from an iridium hydride complex to unactivated olefins. *Chem. Sci.* **11**, 8582–8594 (2020).
49. Kean, K. M. & Karplus, P. A. Structure and role for active site lid of lactate monooxygenase from *Mycobacterium smegmatis*. *Protein Sci.* **28**, 135–149 (2019).
50. Wayner, D. D. M., McPhee, D. J. & Griller, D. Oxidation and reduction potentials of transient free radicals. *J. Am. Chem. Soc.* **110**, 132–137 (1988).
51. Mandal, M., Buss, J. A., Chen, S.-J., Cramer, C. J. & Stahl, S. S. Mechanistic insights into radical formation and functionalization in copper/N-fluorobenzenesulfonimide radical-relay reactions. *Chem. Sci.* **15**, 1364–1373 (2024).
52. Mayhew, S. G. The effects of pH and semiquinone formation on the oxidation–reduction potentials of flavin mononucleotide. *Eur. J. Biochem.* **265**, 698–702 (1999).
53. Zhang, B. et al. Enantioselective cyanofunctionalization of aromatic alkenes via radical anions. *J. Am. Chem. Soc.* **146**, 1410–1422 (2024).
54. Mirdita, M. et al. ColabFold: making protein folding accessible to all. *Nat. Methods* **19**, 679–682 (2022).
55. Jurrus, E. et al. Improvements to the APBS biomolecular solvation software suite. *Protein Sci.* **27**, 112–128 (2018).


**Publisher's note** Springer Nature remains neutral with regard to jurisdictional claims in published maps and institutional affiliations.

Springer Nature or its licensor (e.g. a society or other partner) holds exclusive rights to this article under a publishing agreement with the author(s) or other rightsholder(s); author self-archiving of the accepted manuscript version of this article is solely governed by the terms of such publishing agreement and applicable law.

© Merck & Co., Inc., Rahway, NJ, USA and its affiliates & Princeton University, under exclusive licence to Springer Nature Limited 2024

## Data availability

The data that support the findings of this study are available from the corresponding author upon reasonable request.

**Acknowledgements** F.C.R. thanks the Swiss National Science Foundation (SNSF) for their funding as part of a Postdoc.Mobility Grant (no. P500PN 202708). This work was supported by the National Institutes of Health (NIGMS R01GM127703). We thank A. Brown and K. Berger for help with the DFT calculations, Y. Ouyang and S. Bender for helpful mechanistic discussions and A. Mattevi for helpful insights into Baeyer–Villiger mono-oxygenases.

**Author contributions** T.K.H. and F.C.R. conceived the work. All authors designed the experiments. F.C.R. performed the enzyme identification and evolution. F.C.R. and A.R.-S. synthesized the starting materials and F.C.R. tested the enzymatic activity. A.R.S. performed the kinetic studies and F.C.R. and A.R.-S. performed the spectroscopic studies. C.M.J. performed the MD studies. F.C.R. performed the DFT studies. T.K.H. and F.C.R. prepared the manuscript.

**Competing interests** The authors declare no competing interests.

**Additional information**
**Supplementary information** The online version contains supplementary material available at https://doi.org/10.1038/s41586-024-08138-w.
**Correspondence and requests for materials** should be addressed to Todd K. Hyster.
**Peer review information** *Nature* thanks Hans Bunzel, Elaine O'Reilly and the other, anonymous, reviewer(s) for their contribution to the peer review of this work.
**Reprints and permissions information** is available at http://www.nature.com/reprints.